The Journal *of* Immunology

This information is current as of July 22, 2021.

Deficiency of the AIM2–ASC Signal Uncovers the STING-Driven Overreactive Response of Type I IFN and Reciprocal Depression of Protective IFN- γ Immunity in Mycobacterial Infection

Shanshan Yan, Hongbo Shen, Qiaoshi Lian, Wenlong Jin, Ronghua Zhang, Xuan Lin, Wangpeng Gu, Xiaoyu Sun, Guangxun Meng, Zhigang Tian, Zheng W. Chen and Bing Sun

Supplementary Material	http://www.jimmunol.org/content/suppl/2017/12/18/jimmunol.1701177.DCSupplemental
References	This article **cites 39 articles**, 8 of which you can access for free at: http://www.jimmunol.org/content/200/3/1016.full#ref-list-1

Why *The JI*? Submit online.

- **Rapid Reviews! 30 days*** from submission to initial decision

- **No Triage!** Every submission reviewed by practicing scientists

- **Fast Publication!** 4 weeks from acceptance to publication

average

Subscription	Information about subscribing to *The Journal of Immunology* is online at: http://jimmunol.org/subscription
Permissions	Submit copyright permission requests at: http://www.aai.org/About/Publications/JI/copyright.html
Email Alerts	Receive free email-alerts when new articles cite this article. Sign up at: http://jimmunol.org/alerts

Errata   An erratum has been published regarding this article. Please see next page or:
/content/204/2/472.full.pdf

Deficiency of the AIM2–ASC Signal Uncovers the STING-Driven Overreactive Response of Type I IFN and Reciprocal Depression of Protective IFN-γ Immunity in Mycobacterial Infection

Shanshan Yan,[*,†] Hongbo Shen,[‡,1] Qiaoshi Lian,[†,§] Wenlong Jin,[‡] Ronghua Zhang,[†] Xuan Lin,[‡] Wangpeng Gu,[*,†] Xiaoyu Sun,[‡] Guangxun Meng,[‡] Zhigang Tian,[*] Zheng W. Chen,[¶,1] and Bing Sun[†,1]

The nucleic acids of *Mycobacterium tuberculosis* can be detected by intracellular DNA sensors, such as cyclic GMP-AMP synthase and absent in melanoma 2 (AIM2), which results in the release of type I IFN and the proinflammatory cytokine IL-1β. However, whether cross-talk occurs between AIM2–IL-1β and cyclic GMP-AMP synthase–type I IFN signaling upon *M. tuberculosis* infection in vivo is unclear. In this article, we demonstrate that mycobacterial infection of AIM2$^{-/-}$ mice reciprocally induces overreactive IFN-β and depressive IFN-γ responses, leading to higher infection burdens and more severe pathology. We also describe the underlying mechanism whereby activated apoptosis-associated speck-like protein interacts with a key adaptor, known as stimulator of IFN genes (STING), and inhibits the interaction between STING and downstream TANK-binding kinase 1 in bone marrow–derived macrophages and bone marrow–derived dendritic cells, consequently reducing the induction of type I IFN. Of note, apoptosis-associated speck-like protein expression is inversely correlated with IFN-β levels in PBMCs from tuberculosis patients. These data demonstrate that the AIM2–IL-1β signaling pathway negatively regulates the STING–type I IFN signaling pathway by impeding the association between STING and TANK-binding kinase 1, which protects the host from *M. tuberculosis* infection. This finding has potential clinical significance. *The Journal of Immunology*, 2018, 200: 1016–1026.

T uberculosis (TB) has existed for millennia and remains a major global health problem that now ranks above HIV/AIDS as a leading cause of death from infectious disease. One third

*School of Life Sciences, University of Science and Technology of China, Hefei 230022, China; †State Key Laboratory of Cell Biology, CAS Center for Excellence in Molecular Cell Science, Shanghai Institute of Biochemistry and Cell Biology, Chinese Academy of Sciences, University of Chinese Academy of Sciences, Shanghai 200031, China; ‡CAS Key Laboratory of Molecular Virology and Immunology, Institute Pasteur of Shanghai, Chinese Academy of Sciences, Shanghai 200031, China; §University of Chinese Academy of Sciences, Beijing 100049, China; and ¶Department of Microbiology and Immunology, Center for Primate Biomedical Research, University of Illinois College of Medicine, Chicago, IL 60612

[1]H.S., Z.W.C., and B.S. are the senior authors and contributed equally to this work.

ORCIDs: 0000-0003-4634-4661 (G.M.); 0000-0003-2545-5282 (B.S.).

Address correspondence and reprint requests to Prof. Bing Sun, State Key Laboratory of Cell Biology, CAS Center for Excellence in Molecular Cell Science, Shanghai Institute of Biochemistry and Cell Biology, Shanghai Institutes of Biological Sciences, Chinese Academy of Sciences, University of Chinese Academy of Sciences, 320 Yue Yang Road, Shanghai 200031, China. E-mail address: bsun@sibs.ac.cn

The online version of this article contains supplemental material.

Abbreviations used in this article: AIM2, absent in melanoma 2; ASC, apoptosis-associated speck-like protein; BCG, bacillus Calmette–Guérin; BMDC, bone marrow–derived dendritic cell; BMDM, bone marrow–derived macrophage; cGAMP, cyclic GMP-AMP; cGAS, cyclic GMP-AMP synthase; GD, genomic DNA; HA, hemagglutinin; IRF3, IFN regulatory factor 3; ISD, IFN stimulatory DNA; PAMP, pathogen-associated molecular pattern; poly(dA:dT), poly(deoxyadenylic-thymidylic) acid; poly(I:C), polyinosinic-polycytidylic acid; STING, stimulator of IFN genes; TB, tuberculosis; TBK1, TANK-binding kinase 1; WT, wild-type.

of the world's population has been infected with TB. Of these infected people, 1.4 million died in 2015 (1). The lack of effective vaccines and sensitive diagnostic methods has affected global control of the TB epidemic. The immune system plays critical roles in controlling TB infection (2). Therefore, the incompletely characterized immune responses of TB patients must be explored to enable the establishment of new vaccines, diagnostics, and treatments.

The innate immune system recognizes pathogen signatures, known as pathogen-associated molecular patterns (PAMPs), to sense pathogenic invasion by using germline-encoded pattern recognition receptors; the detection of foreign nucleic acids acting as classical PAMPs has evolved as a fundamental mechanism of host defense (3). *Mycobacterium tuberculosis* can activate the DNA-dependent cytosolic surveillance pathway (4). When the immune system of the host senses the invasion of *M. tuberculosis*, the DNA sensor cyclic GMP-AMP synthase (cGAS) binds to the genomic DNA (GD) of the pathogen and catalyzes the production of cyclic GMP-AMP (cGAMP). cGAMP then activates a downstream adaptor molecule known as stimulator of IFN genes (STING), which promotes the translocation of STING from the endoplasmic reticulum to the perinuclear microsomal compartments. After STING activation, downstream molecules, TANK-binding kinase 1 (TBK1) and IFN regulatory factor 3 (IRF3), are activated, which ultimately results in the release of type I IFN (5–7).

Although type I IFN plays an important role in the antiviral immune response, studies of patients and mice have highlighted the detrimental role of IFN-α/β during *M. tuberculosis* infection (8). Many reports have demonstrated that patients with active TB exhibit a prominent IFN-α/β–inducible transcription signature that correlates with the extent of radiographic disease and

diminishes with successful treatment (9–11). Furthermore, disruption of the IFN-α/β receptor gene or Ab-mediated neutralization of IFN-α/β increases the survival rate of infected mice relative to wild-type (WT) control mice (12). Increased infection severity has also been demonstrated through direct instillation of IFN-α/β into the lungs and through administration of a TLR3 ligand that induces IFN-α/β (13, 14).

In addition to detection by the STING–type I IFN signaling pathway, GD of *M. tuberculosis* can be detected by absent in melanoma 2 (AIM2), another important DNA sensor. When AIM2 senses abnormal cytoplasmic DNA, it associates with adaptor molecules known as apoptosis-associated speck-like protein (ASC) and inactivated procaspase-1, forming a complex called the AIM2 inflammasome, which induces the production of proinflammatory cytokines, such as IL-1β and IL-18 (15–17). Unlike type I IFN, proinflammatory cytokines are conducive to the antibacterial immune response. For example, IL-1α/β–knockout mice develop significantly larger granulomatous lesions than WT mice postinfection with H37Rv (18). Furthermore, IL-1R$^{-/-}$ mice show increased mortality and enhanced mycobacterial outgrowth in their lungs and distant organs compared with normal mice (19). Additionally, the low production of IL-1β and IL-18 in AIM2$^{-/-}$ mice increases susceptibility to *M. tuberculosis* infection (20).

Because the balance between AIM2–IL-1β and cGAS–type I IFN signaling governs the outcome of *M. tuberculosis* infection, it is important to address whether there is a cross-talk between these two signaling pathways during *M. tuberculosis* infection in vivo. In this study, we demonstrated that the overreactive IFN-β and less protective IFN-γ responses were induced in AIM2$^{-/-}$ mice upon mycobacterial infection, leading to higher infection burdens and more severe pathology. Furthermore, our mechanistic study indicated that activated ASC interacted with STING and blocked the association between TBK1 and STING, thereby inhibiting the induction of type I IFN. Our study reveals a novel mechanism that is involved in the cross-talk between the AIM2–IL-1β and STING–type I IFN pathways during mycobacterial infection. This mechanism may have potential applications in the clinic.

Materials and Methods

Mice

AIM2$^{-/-}$ and Caspase-1$^{-/-}$ mice were obtained from The Jackson Laboratory. ASC$^{-/-}$ mice have been described previously (21). C57BL/6 WT mice were purchased from the Shanghai Laboratory Animal Center. All mice were housed in specific pathogen–free conditions.

Reagents

Polyinosinic-polycytidylic acid [poly(I:C)] and IFN stimulatory DNA (ISD) were purchased from Invitrogen. Poly(deoxyadenylic-thymidylic) acid [poly(dA:dT)], cGAMP, and LPS were purchased from Sigma. Genomic DNA from the spleens of C57BL/6 mice was obtained in-house using a DNeasy Blood & Tissue Kit (69504; QIAGEN). 150mer dsDNA was amplified by PCR from the β-actin gene and purified using a Plus DNA Clean/Extraction Kit (DP034P-300; GeneMark). The following Abs were used for the immunoblotting analysis or immunoprecipitation: anti-HA (CO-MMS-101R; Covance), anti-Flag (F3165; Sigma), anti–c-Myc (A02060; AmyJet Scientific), anti-STING (3337; Cell Signaling Technology), anti-TBK1 (3013S; Cell Signaling Technology), anti-phosphorylated TBK1 (5483S; Cell Signaling Technology), anti-IRF3 (sc-9082; Santa Cruz Biotechnology), and anti-phosphorylated IRF3 (4947s; Cell Signaling Technology). Anti-ASC Ab was produced by immunization of rabbits with ASC expressed by *Escherichia coli*. The following Abs were used for confocal microscopy: Alexa Fluor 488 goat anti-mouse IgG (A11034; Molecule Probes) and Cy3 goat anti-rabbit IgG (115-165-146; Jackson ImmunoResearch). Lipofectamine 2000 was obtained from Invitrogen. X-tremeGENE DNA transfection reagent was purchased from Roche. TurboFect Transfection Reagent was purchased from Thermo Fisher. A Dual-Luciferase Reporter Assay System was obtained from Promega. Protein A/G PLUS-Agarose Immunoprecipitation Reagent was purchased from Santa Cruz Biotechnology. Anti-HA and anti-FLAG beads were purchased from Sigma. Murine IFN-β (439408; BioLegend) and mouse IFN-r (P105796; R&D Systems) ELISA kits were used. All ASC truncations were generated by PCR and subcloned into a pcDNA3 vector. The other plasmids were generated or obtained as we described previously (22).

Mycobacteria strain and culture conditions

Mycobacterium bovis bacillus Calmette-Guérin (BCG) Danish strain (ATCC 35733) was grown at 37°C in Middlebrook 7H9 broth or on Middlebrook 7H10 agar (both from Difco) supplemented with 10% oleic acid–albumin–dextrose–catalase–enriched Middlebrook (BD), 0.2% glycerol, and 0.05% Tween-80 for 3–4 wk. CFU of bacteria were counted.

Mouse infection

WT, AIM2$^{-/-}$, and Caspase-1$^{-/-}$ mice were challenged by tail vein injection with 4×10^7 CFU attenuated *M. bovis* (BCG) in 200 μl of PBS per mouse (4–6 wk of age) at 0, 20, 30, and 40 d. Fifty days after the first injection, mice were sacrificed, and samples were harvested. The amounts of IFN-β and IFN-γ in the serum were detected as soon as possible. The lungs were homogenized in PBS and plated on 7H11 agar to determine the bacterial burden.

Histopathology analysis

The lungs of each mouse were excised and cut into two pieces: one was subjected to CFU counting, and one was fixed in a 4% neutral-buffered paraformaldehyde solution for 24 h. After paraffin embedding, a series of sections with a thickness of 4–7 μm were cut and stained with H&E using standard methods, and images were obtained using a microscope (BX51WI; Olympus).

Cell culture, transfection, and stimulation

Generation of bone marrow–derived macrophages (BMDMs) and bone marrow–derived dendritic cells (BMDCs) has been described previously (22). Briefly, bone marrow cells were flushed from the femurs and tibias of mice and subsequently depleted of RBCs with RBC lysing buffer. BMDCs were cultured at 1.5×10^6 cells per well in 24-well plates in RPMI 1640 supplemented with 10% (v/v) FBS, 20 ng/ml murine GM-CSF, and 2 mM L-glutamine. BMDMs were cultured at 3×10^6 cells per well in 12-well plates in DMEM supplemented with 10% (v/v) FBS and 20 ng/ml murine M-CSF. Fresh medium was added every 2 d. BMDCs and BMDMs were collected for further experiments on days 7 and 5, respectively. MEFs (American Type Culture Collection), RAW264.7 cells (Cell Bank of Chinese Academy of Sciences), and HEK293T cells (Cell Bank of Chinese Academy of Sciences) were cultured in humidified 5% CO_2 at 37°C in DMEM supplemented with 10% (v/v) FBS, 0.5% penicillin (100 U/ml), and streptomycin (100 U/ml). X-tremeGENE was used for transient transfections of plasmid DNA into MEFs. Transfections of HEK293T cells were performed using TurboFect. Poly(dA:dT), ISD, cGAMP, GD, 150mer dsDNA, and poly(I:C) were transfected using Lipofectamine 2000, according to the manufacturer's recommendations.

Generation of RAW-GFP and RAW-ASC cells

ASC was cloned into MSCV–IRES–GFP and transfected with pCMV/ VSV-G and pKF3-RSV/Gag-Pol into HEK293T cells by calcium phosphate transfection. After 6 and 24 h, the medium was replaced with fresh DMEM containing 10% FBS. Forty-eight hours after the transfections, the retroviral supernatants were harvested, supplemented with 16 μg/ml Polybrene, and used to infect RAW264.7 cells. The cell culture plates were centrifuged at $1800 \times g$ for 90 min at room temperature. After 12 h of incubation at 37°C, the retroviruses were removed, and the cells were cultured in fresh medium for another 12 h. Finally, the cells were collected to sort GFP$^+$ cells using a FACSAria II (BD Biosciences) for culture and further experiments.

Real-time PCR

RNA that was extracted from the cells was reverse transcribed using a Prime Script RT Master Mix Kit (Takara), and quantitative PCR analysis was performed on an ABI Q6. All gene expression data are relative to HPRT. The following primers were used for PCR: IFN-β sp 5′-CCTGGAGCAGCT-GAATGGAA-3′, as 5′-TTGAAGTCCGCCCTGTAGGT-3′ and HPRT sp 5′-TGCTCGAGATGTCATGAAGGAG-3′, as 5′-CAGAGGGCCACAATGTGATG-3′.

Immunoprecipitation and immunoblotting analysis

Immunoprecipitation and immunoblotting procedures have been described (22). Briefly, for exogenous coimmunoprecipitation experiments, HEK293T cells

were transfected with various combinations of plasmids. Twenty-four hours after the transfections, cell lysates were prepared in lysis buffer and incubated with hemagglutinin (HA) beads overnight at 4˚C. Complexes were washed three times with lysis buffer and analyzed by immunoblotting. For the endogenous coimmunoprecipitation experiments, BMDCs were stimulated with poly(dA:dT) for 6 h. Lysates were incubated with anti-ASC Ab or rabbit IgG Ab and analyzed by immunoblotting with anti-STING Ab.

Confocal microscopy

MEFs were transfected with the HA–ASC and Flag–STING plasmids. After 24 h, the cells were collected and seeded onto glass coverslips in 24-well plates overnight before stimulation with 1 μg/ml poly(dA:dT) or were left unstimulated for 4 h. After stimulation, cells were fixed with 4% paraformaldehyde in PBS, permeabilized with Triton X-100, and blocked with 1% BSA in PBS. Cells were stained with anti-HA mouse Ab and anti-FLAG rabbit Ab, followed by Cy3-conjugated anti-rabbit Ab and Alexa Fluor 488–conjugated anti-mouse IgG Ab, and counterstained for nucleic acids with DAPI. Finally, fluorescence images were captured with a Leica TCS SP5 MP laser confocal microscope.

Luciferase reporter gene assay

MEFs were cotransfected with an IFN-β, ISRE, or IFN-α4 luciferase reporter plasmid, a *Renilla* luciferase plasmid as an internal control, and the indicated expression plasmids. An empty control vector was added to equalize the amount of DNA added to each well of cells. Twenty-four hours after the transfection, cells were lysed, and the reporter activity was measured using a Dual-Luciferase Reporter Assay System (Promega).

Patients

PBMCs were isolated from EDTA-treated blood by Ficoll-Paque Plus density gradient centrifugation. TB patients were enrolled from the Shanghai Pulmonary Hospital (Shanghai, China). Age- and gender-matched healthy volunteers were recruited into this study who had no history or evidence of TB (negative T-SPOT for TB). None of the participants showed evidence of acute infection with hepatitis B virus, hepatitis C virus, HIV, or other infectious agent or of cancers. Informed consent was obtained from all participants.

Ethics statement

All experiments were carried out according to the National Institutes of Health *Guide for the Care and Use of Laboratory Animals* with the approval of the Institutional Animal Care and Use Committee of the Institute Pasteur of Shanghai and the Institutional Animal Care and Use Committee of the Shanghai Institute of Biochemistry and Cell Biology, Chinese Academy of Sciences (approval number SIBCB-S303-1608-025). Protocols for the use of human blood samples for in vitro experimental procedures were evaluated and approved by the Institutional Review Board for Human Subjects Research and the Institutional Biosafety Committee at the Institute Pasteur of Shanghai, Shanghai Pulmonary Hospital. All studies were conducted in accordance with the amended Declaration of Helsinki (International Conference on Harmonisation-Good Clinical Practice) and consistent with the guidelines of the Office for Human Research Protections. All subjects were adults and signed written informed consent forms.

Statistical analysis

Statistical comparisons between the different treatments were performed using the unpaired Student *t* test. Correlations were performed using the Pearson test. Statistically significant *p* values are noted in the figures.

Results

Mycobacterial infection of AIM2−/− mice reciprocally induces overreactive IFN-β and depressive IFN-γ responses, leading to higher infection burdens and more severe pathology

To explore whether the AIM2–IL-1β signaling pathway affected the STING–type I IFN signaling pathway during mycobacterial infection in vivo, AIM2−/− (Supplemental Fig. 1A, 1B) and WT mice were infected with attenuated *M. bovis* (BCG) (Fig. 1A), and their levels of protective IFN-γ, bacilli-enhancing IFN-β, and BCG infection burdens, as well as the severity of tissue pathology, were assessed. Caspase-1−/− mice (Supplemental Fig. 1D) were

used as the control for AIM2-deficient mice in the context of BCG infection based on the involvement of the AIM2/ASC/caspase-1 inflammasome complex that is capable of regulating TB infection (20). We used BCG infection for two reasons: 1) BCG infection and vaccination reportedly induce a strong IFN-γ response and immunity (23), and potential overproduction of IFN-β in infected AIM2−/− mice may antagonize IFN-γ, leading to a loss of immunity or a different outcome and 2) high levels of mycobacterial DNA can be generated by repeated BCG infections, making it possible to optimally uncover the DNA sensor–driven IFN-β function and mechanisms in vivo during repeated BCG infections. Moreover, BCG could readily allow us to conduct proof-of-concept and mechanistic studies at Animal Biosafety Level 2, without the need for expensive or highly regulated Animal Biosafety Level 3 facilities. Interestingly, serum IFN-β levels were significantly higher in AIM2−/− mice than in WT control mice (Fig. 1B), suggesting that AIM2 deficiency might enhance the induction of type I IFN during mycobacterial infection in vivo. Surprisingly, BCG infection of AIM2−/− mice with overreactive IFN-β almost shut down the protective IFN-γ response, whereas WT mice exhibited robust IFN-γ production in the serum (Fig. 1B). The strong inverse correlation between IFN-β and IFN-γ in WT and AIM2−/− mice suggested that IFN-β overproduction might help to antagonize the protective IFN-γ response in mycobacterial infection (24). In contrast to AIM2−/− mice, Caspase-1−/− controls did not exhibit significantly higher serum IFN-β levels than WT mice after BCG infection, whereas AIM2−/− and Caspase-1−/− mice produced less IL-1β than WT animals (Supplemental Fig. 2). Notably, BCG-infected AIM2−/− mice showed significantly higher levels of mycobacterial burdens in their lung tissues compared with WT and Caspase-1−/− controls (Fig. 1C). Moreover, BCG infection of AIM2−/− mice caused a more striking splenomegaly compared with that of WT and Caspase-1−/− mice (Fig. 1D). Consistently, BCG-infected AIM2−/− mice showed more severe lung pathology, which was characterized by apparent infiltration of inflammatory exudates/cells in the lung tissues, compared with WT and Caspase-1−/− controls (Fig. 1E). Taken together, these results demonstrated that BCG infection of AIM2−/− mice reciprocally induced overreactive IFN-β and depressive IFN-γ responses, leading to higher infection burdens and more severe pathology compared with WT and Caspase-1−/− controls.

AIM2 deficiency enhances STING-driven type I IFN signaling upon BCG infection or stimulation with various DNA forms in BMDCs and BMDMs

We aimed to dissect the signaling cascade whereby AIM2 deficiency during BCG infection led to an overreactive IFN-β response and exacerbated pathology. Because macrophages and dendritic cells in the lungs are major target cells for *M. tuberculosis* and BCG during the early stage of infection (2), we used BMDMs and BMDCs for the mycobacterial DNA–mediated signaling studies. We first examined whether BCG, similar to *M. tuberculosis* bacilli, could induce IFN-β production through activation of the cGAS–STING–TBK1 signaling pathway. Indeed, BCG behaved like *M. tuberculosis* in terms of cGAS-driven production of IFN-β, which was reflected by a significant reduction in BCG-stimulated production of IFN-β after cGAS was knocked down in BMDCs or BMDMs (Fig. 2A). The in vivo data led us to speculate that the AIM2 inflammasome signaling pathway might inhibit the production of IFN-β upon BCG infection. To test this speculation, BMDCs and BMDMs from WT and AIM2−/− mice were stimulated with BCG in culture and assessed for an IFN-β response. We found that BCG infection of AIM2-deficient BMDCs
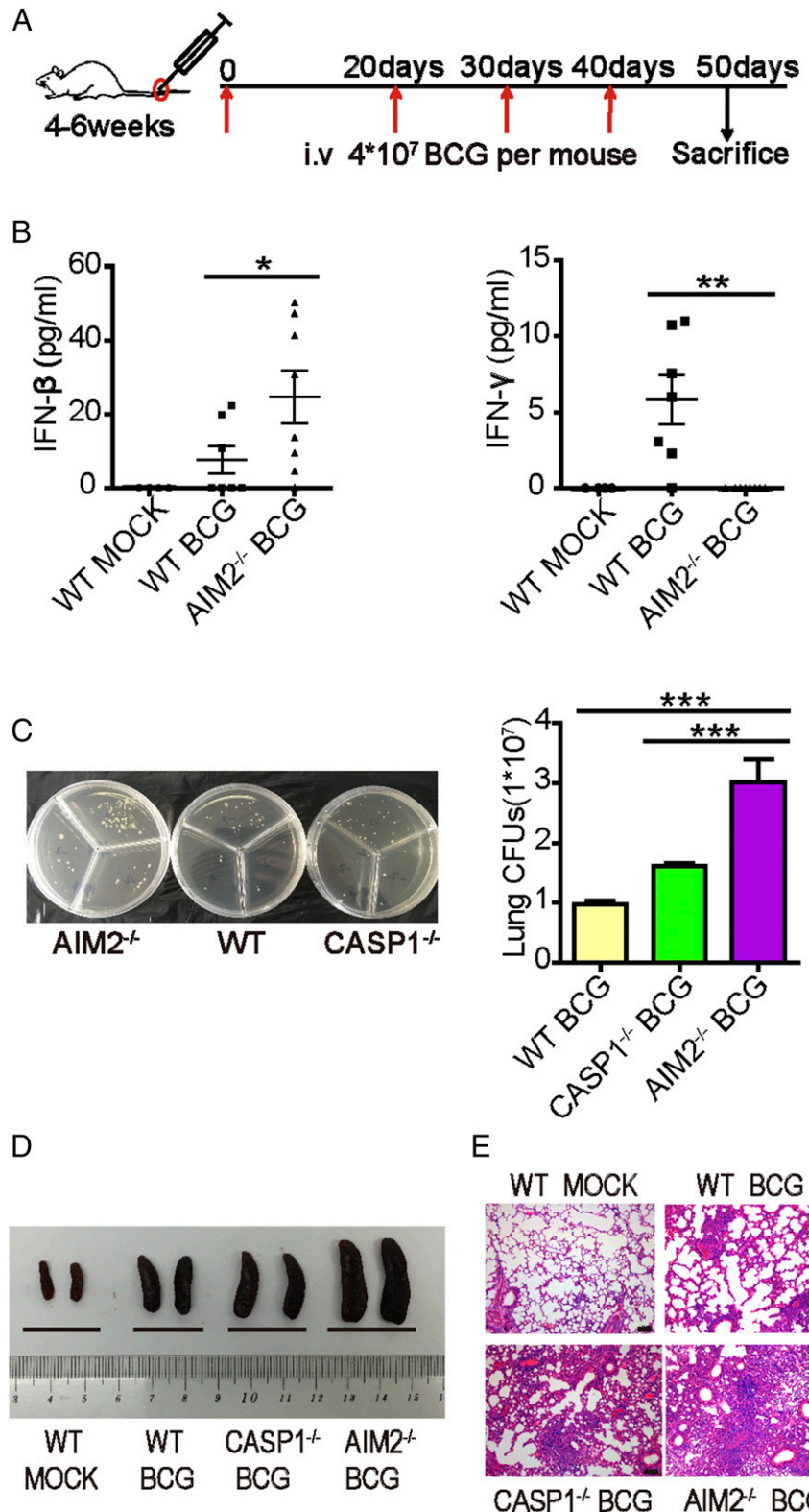
FIGURE 1. AIM2-mediated inhibition of IFN-β production is necessary for controlling *M. bovis* (BCG) infection in vivo. WT, AIM2$^{-/-}$, and Caspase-1$^{-/-}$ mice were infected with 4×10^7 CFU BCG four times. (**A**) Schematic diagram of the infection with BCG. (**B**) Levels of IFN-β and IFN-γ in the sera of WT and AIM2$^{-/-}$ mice, with or without BCG infection. (**C**) Bacterial CFU counts in the homogenates of lungs from BCG-infected WT, AIM2$^{-/-}$, and Caspase-1$^{-/-}$ mice in a representative of two independent experiments. Five to six mice per group were used in the experiments, and two AIM2$^{-/-}$ mice died with extremely high CFU counts (outlier not included). Similar significance trends for comparisons between AIM2$^{-/-}$ and control groups were seen in the other experiment. (**D**) Gross pathology features of the spleens of two representative mice from each group infected with BCG. (**E**) Histopathology of the lungs from mice infected with BCG. Sections were stained with H&E and assessed. Scale bars, 100 μm. Data are representative of at least two independent experiments. The results are shown as mean ± SEM. *$p < 0.05$, **$p < 0.01$, ***$p < 0.001$, Student *t* test.

and BMDMs also upregulated IFN-β (Fig. 2B), thus recapitulating the in vivo finding in BCG-infected AIM2$^{-/-}$ mice (Fig. 1B). To examine this further, we determined whether other common forms of DNA, such as poly(dA:dT) and murine-derived GD, promoted IFN-β production based on a similar effect that was previously reported with tumor-derived DNA (25). We observed that stimulation of AIM2-deficient BMDCs and BMDMs with GD and poly(dA:dT), but not with the RNA sensor ligand poly(I:C),

similarly enhanced the production of IFN-β and related cytokines (i.e., IFN-α1 and IP-10) (Fig. 2C, Supplemental Fig. 3A, 3B). Moreover, the enhancing effect in the absence of AIM2 was dependent on the DNA concentration at the IFN-β mRNA and protein levels (Fig. 2D). These data suggested that the AIM2 inflammasome signaling pathway negatively regulated STING-driven production of type I IFN upon stimulation with BCG infection or various DNA forms.
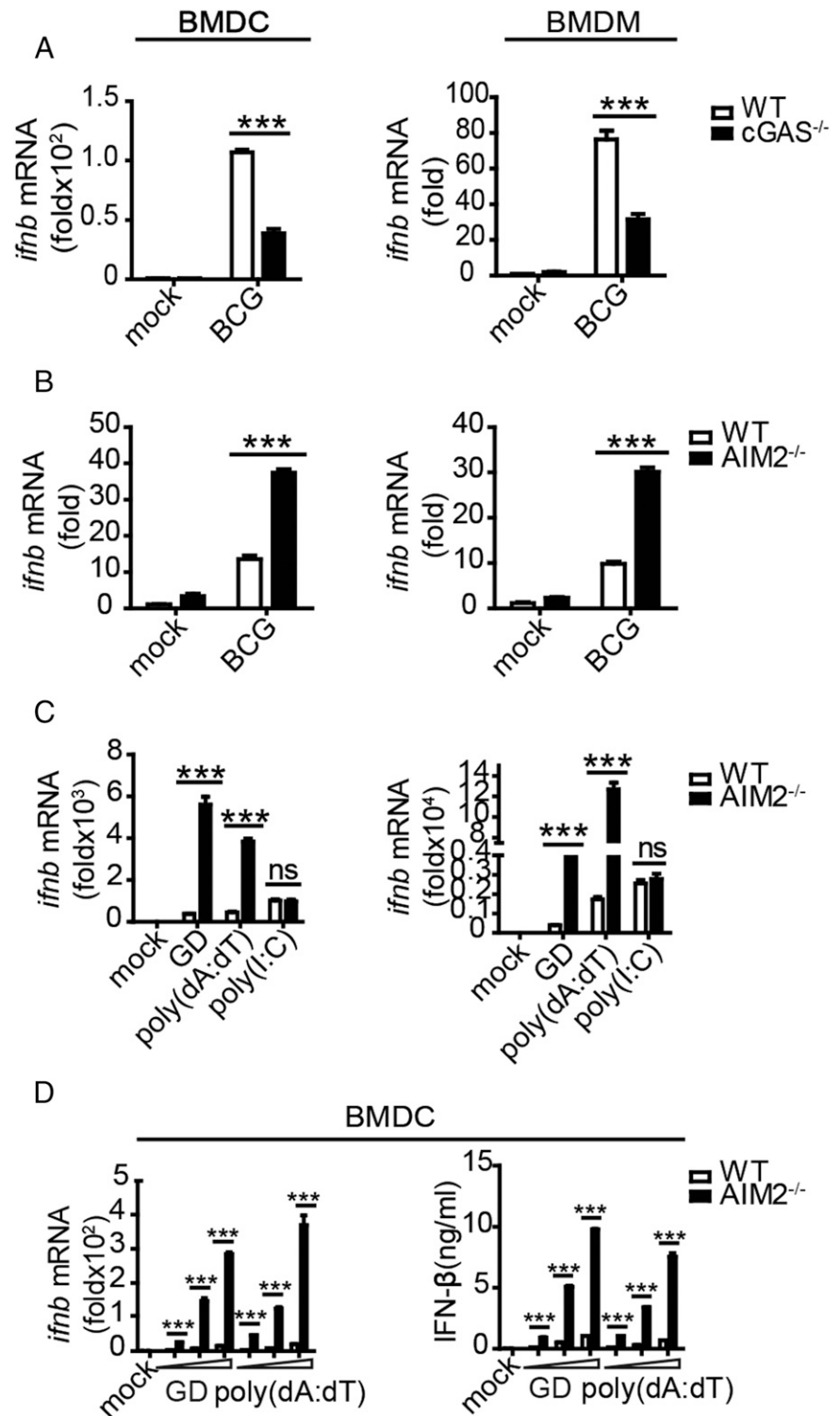
FIGURE 2. AIM2 deficiency enhances the induction of IFN-β upon BCG infection or stimulation with various DNA forms in BMDCs and BMDMs. BMDCs and BMDMs from WT, cGAS$^{-/-}$ (**A**), and AIM2$^{-/-}$ mice (**B**) were infected with BCG (multiplicity of infection = 10) for 6 h, and IFN-β transcripts were measured by quantitative real-time PCR (qRT-PCR). (**C**) BMDCs and BMDMs from WT and AIM2$^{-/-}$ mice were stimulated with GD (1.5 μg/ml), poly(dA:dT) (1.5 μg/ml), and poly(I:C) (2 μg/ml), and IFN-β was measured by qRT-PCR 8 h after transfections. (**D**) BMDCs from WT and AIM2$^{-/-}$ mice were stimulated with 0.5, 1, or 2 μg/ml DNA for 10 h, and IFN-β was measured by qRT-PCR and ELISA. Data are representative of at least three independent experiments. The results are shown as mean ± SEM. ***$p < 0.001$, Student t test. ns, not significant.

Activated ASC negatively regulates the production of IFN-β

We examined whether AIM2-related inhibition of IFN-β induction in response to stimulation with BCG and various DNA forms was dependent on the AIM2 sensor itself or on the downstream inflammasome signaling of AIM2 in the context of the STING pathway. Interestingly, when STING-activating ISD (a 45-bp DNA) and cGAMP (the catalytic product of cGAS) were used to stimulate WT and AIM2$^{-/-}$ BMDCs and BMDMs, no difference in the induction of IFN-β was observed (Fig. 3A, 3B). Given that ISD and cGAMP activate only STING signaling and that poly(dA:dT) stimulates STING signaling and AIM2 inflammasome signaling

(Supplemental Fig. 4A) (26), we speculated that the AIM2 inflammasome signaling pathway might be involved in the negative regulation of IFN-β. To identify potential regulatory molecules in the AIM2 inflammasome signaling pathway, we used B-form DNA, poly(dA:dT), or GD to activate downstream molecules in BMDCs and BMDMs from WT, AIM2$^{-/-}$, ASC$^{-/-}$ (Supplemental Fig. 1C), and Caspase-1$^{-/-}$ mice. We found that IFN-β was increased only 2-fold in caspase-1–deficient cells compared with WT cells. In contrast, >10-fold increases in IFN-β were similarly observed in AIM2-deficient and ASC-deficient cells at the mRNA and protein levels (Fig. 3C–F). Notably, these results were consistent with
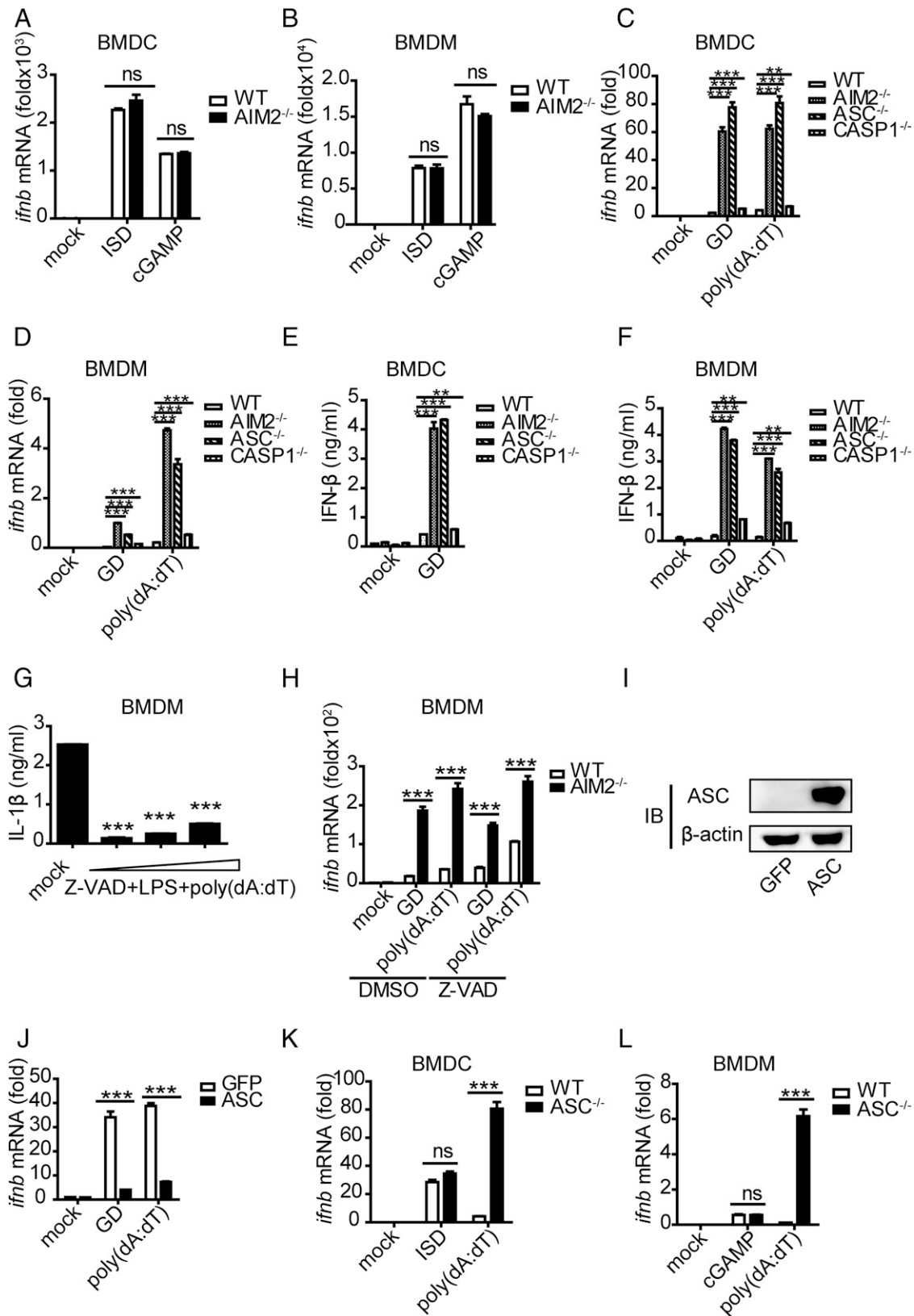
FIGURE 3. The activated form of ASC performs an inhibitory role on IFN-β upon DNA ligand stimulation. (**A** and **B**) BMDCs and BMDMs isolated from WT and AIM2$^{-/-}$ mice were stimulated with ISD (1.5 μg/ml) and cGAMP (4 μg/ml), and IFN-β was measured by quantitative real-time PCR (qRT-PCR) 8 h after transfection. (**C** and **D**) BMDCs and BMDMs isolated from WT, AIM2$^{-/-}$, ASC$^{-/-}$, and Caspase-1$^{-/-}$ mice were stimulated with GD (1.5 μg/ml) and poly(dA:dT) (1.5 μg/ml), and IFN-β was measured by qRT-PCR 10 h after transfection. (**E** and **F**) BMDCs and BMDMs isolated from WT, AIM2$^{-/-}$, ASC$^{-/-}$, and Caspase-1$^{-/-}$ mice were stimulated with GD (1.5 μg/ml) and poly(dA:dT) (1.5 μg/ml), and IFN-β was measured by ELISA 10 h after transfection. (**G**) BMDMs isolated from WT mice were stimulated with different concentrations of a caspase inhibitor (Z-VAD-FAM) for 1 h and then stimulated with LPS for 2 h before being stimulated with poly(dA:dT) (1.5 μg/ml); IL-1β was measured by ELISA 6 h after transfection. (**H**) BMDMs isolated from WT and AIM2$^{-/-}$ mice were stimulated with DMSO or a caspase inhibitor (Z-VAD-FAM) for 1 h and then *(Figure legend continues)*

previous reports (25). To confirm the role of caspase-1 in IFN-β production, we incubated WT and AIM2$^{-/-}$ BMDCs with Z-VAD-FAM, a caspase inhibitor, and then stimulated them with DNA. A concentration of 50 μM was chosen as the final working concentration based on its inhibitory efficiency of IL-1β (Fig. 3G). Although Z-VAD-FAM–mediated inhibition in WT BMDMs moderately upregulated IFN-β, it did not have a significant impact on the remarkably high levels of IFN-β in AIM2$^{-/-}$ BMDMs (Fig. 3H), suggesting that caspase-1/IL-1β or IL-18 might not be the major negative-regulatory molecules of IFN-β. This prompted the hypothesis that ASC, the upstream molecule, might be responsible for the negative regulation. To test this hypothesis, we overexpressed ASC in RAW264.7 cells and stimulated them with B-form DNA (Fig. 3I, Supplemental Fig. 3C). We found that overexpression of ASC led to marked decreases in IFN-β and a related cytokine, IP-10, compared with RAW264.7 control cells without ASC overexpression (Fig. 3J, Supplemental Fig. 3D). Similar to the setting of AIM2 deficiency, stimulation of the cGAS–STING pathway with ISD or cGAMP in ASC$^{-/-}$ BMDCs did not alter IFN-β production, whereas poly(dA:dT) stimulation in the absence of ASC led to remarkable increases in IFN-β (Fig. 3K, 3L). Taken together, these results suggest that the activated form of ASC may inhibit the production of IFN-β upon DNA stimulation.

Activated ASC targets STING to inhibit the induction of IFN-β

Several DNA sensors, including cGAS, DDX41, and IFI16 (27–29), have been discovered. To examine whether the DNA sensors were the target molecules that were negatively regulated, we stimulated WT and AIM2$^{-/-}$ BMDCs with poly(dA:dT) and synthetic 150mer dsDNA, with recognition of the former being independent of cGAS but recognition of the latter being dependent on cGAS in BMDCs (Fig. 4A, 4B). Induction of IFN-β was strongly increased in AIM2-deficient cells (Fig. 4A, 4B), suggesting that the target was not at the DNA sensor level but was likely downstream of the DNA sensors. To identify the potential target, we performed Western blots to assess activation of two downstream molecules: TBK1 and IRF3. Higher levels of phosphorylated TBK1 and IRF3, which are the activated forms of both molecules, were promoted by AIM2 deficiency relative to control (Fig. 4C). Consistent with the results from BMDCs, overexpression of ASC in RAW264.7 cells inhibited phosphorylation of TBK1 and IRF3 after stimulation with B-form DNA (Fig. 4D), indicating that the target might be upstream of TBK1 and IRF3. Thus, we hypothesized that ASC might target STING to inhibit the production of IFN-β upon DNA stimulation. As shown in Fig. 4E, exogenous expression of ASC indeed inhibited STING-induced IFN-β, ISRE, and IFN-α4 activation in a dose-dependent manner. Taken together, these data showed that activated ASC targeted STING to inhibit DNA-triggered IFN-β induction.

ASC interacts with STING

To investigate how ASC targeting of STING resulted in the DNA-mediated inhibition of IFN-β, coimmunoprecipitation assays were performed. The results showed that ASC interacted with STING when cotransfected into HEK293T cells (Fig. 5A). Trim30α interaction with STING, which we reported previously (22), was used as a positive control. We then verified that endogenous ASC

could indeed interact with STING in BMDCs upon poly(dA:dT) stimulation or BCG infection (Fig. 5B). After 3′HA–ASC and 5′Flag–STING were expressed in HEK293T cells, confocal microscopy revealed that the two proteins colocalized without stimulation and that the colocalization tended to accumulate after poly(dA:dT) stimulation (Fig. 5C). To explore the domains that governed the association between ASC and STING, Flag-tagged full-length STING and two ASC truncations were expressed in HEK293T cells. Coimmunoprecipitation assays showed that only the ASC–CARD domain, which might not affect the activation of ASC, bound to STING (Fig. 5D). This is consistent with findings that activated ASC played the negative-regulatory role. Unlike ASC, STING is a membrane protein that contains four transmembrane domains. After expressing an HA-tagged full-length ASC protein and various STING truncations in HEK293T cells, we found that the N-terminal transmembrane domains (1–136) or the CTT domain (338–378) of STING were required for ASC–STING interaction (Fig. 5E). Because the C terminus (341–379) of STING binds to and activates TBK1 to phosphorylate IRF3 upon DNA ligand stimulation (30), we asked whether the interaction between ASC and STING impeded the interaction between STING and TBK1. To test this supposition, we co-overexpressed STING and TBK1 in HEK293T cells without ASC expression or with gradient ASC expression. The results showed that addition of ASC decreased the association between STING and TBK1 and that the inhibitory effect of ASC on the STING–TBK1 association was gradient dependent (Fig. 5F). Further evidence that ASC could also interact with TBK1 was found for this phenomenon (Fig. 5G). These results indicated that ASC might interfere with the STING–TBK1 association, thus inhibiting the production of IFN-β.

ASC expression is inversely correlated with IFN-β levels in PBMCs of TB

Previous studies have shown that active TB patients exhibit a prominent IFN-α/β–inducible transcription signature. Consistent with these findings, we observed higher IFN-β expression in PBMCs of TB patients compared with healthy donors (Fig. 6A). To identify whether the inhibitory role of ASC on the induction of IFN-β was involved in this phenomenon, we simultaneously measured the expression of ASC. Interestingly, lower expression of ASC was detected in TB patients than in healthy donors (Fig. 6B). Additionally, an inverse correlation was detected between IFN-β levels and ASC levels in TB patients (Fig. 6C), indicating that downregulated expression of ASC might contribute, in part, to the detrimental IFN-α/β–inducible transcriptional signature of TB patients.

Discussion

Although the AIM2–IL-1β and STING–type I IFN signaling pathways are activated by the GD of *M. tuberculosis*, the roles of these pathways are protective (AIM2–IL-1β) and detrimental (STING–type I IFN) to the host against infection. We found that AIM2 deficiency reciprocally induced overreactive IFN-β and depressive IFN-γ responses in vivo, leading to higher infection burdens and more severe pathology. While exploring the potential

stimulated with GD (1.5 μg/ml) and poly(dA:dT) (1.5 μg/ml). IFN-β was measured by qRT-PCR 8 h after transfection. (**I**) Immunoblot of ASC and β-actin in RAW-GFP and RAW-ASC cell lysates. (**J**) RAW-GFP and RAW-ASC cells were stimulated with GD (1.5 μg/ml) and poly(dA:dT) (1.5 μg/ml), and IFN-β was measured by qRT-PCR 8 h after transfection. (**K** and **L**) BMDCs and BMDMs isolated from WT and ASC$^{-/-}$ mice were stimulated with ISD (1.5 μg/ml), cGAMP (4 μg/ml), and poly(dA:dT) (1.5 μg/ml), and IFN-β was measured by qRT-PCR 8 h after transfection. Data are representative of at least two independent experiments. The results are shown as mean ± SEM. **$p < 0.01$, ***$p < 0.001$, Student t test. ns, not significant.
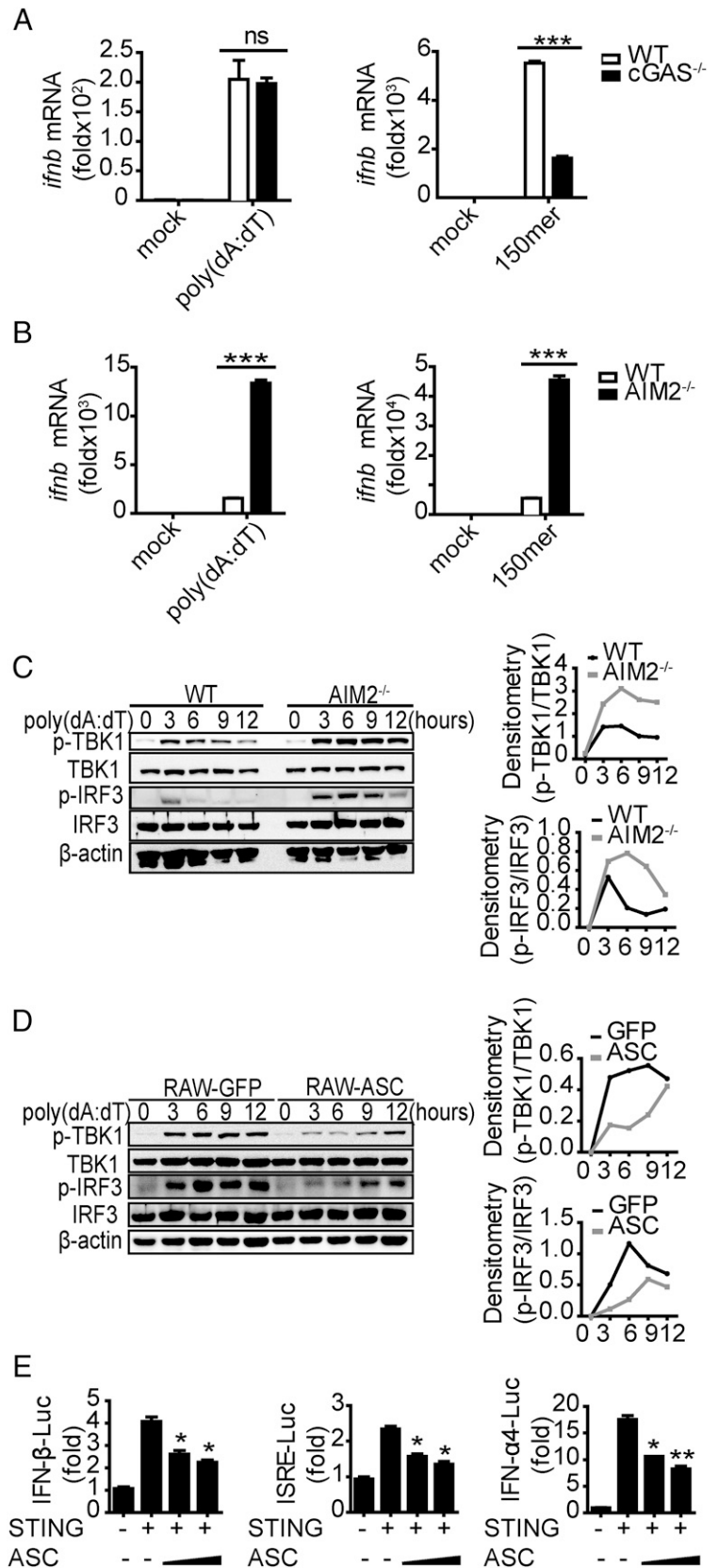
FIGURE 4. ASC negatively regulates IFN-β production by affecting STING function. (**A** and **B**) BMDCs isolated from WT, cGAS$^{-/-}$, and AIM2$^{-/-}$ mice were stimulated with poly(dA:dT) (1.5 µg/ml) and 150mer dsDNA (1.5 µg/ml), and IFN-β was measured by quantitative real-time PCR (qRT-PCR) 8 h after transfection. Immunoblot of p-TBK1, total TBK1, p-IRF3, total IRF3, and β-actin in WT and AIM2$^{-/-}$ BMDC lysates (**C**) or RAW-GFP and RAW-ASC cell lysates (**D**) that were stimulated with poly(dA:dT) (1.5 µg/ml) for the indicated times. (**E**) Luciferase activity of MEFs that were cotransfected with the IFN-β luciferase reporter (0.4 µg/ml), ISRE luciferase reporter (0.4 µg/ml), or IFN-α4 luciferase reporter (0.4 µg/ml) and Flag-STING (0.4 µg/ml) and the empty vector or increasing amounts of HA-ASC. Data are representative of at least two independent experiments. The results are shown as mean ± SEM. *$p < 0.05$, **$p < 0.01$, ***$p < 0.001$, Student t test. ns, not significant.

mechanism behind this phenomenon, we discovered that the interaction between activated ASC and STING impeded the association of STING with its downstream molecule, TBK1, which ultimately inhibited the induction of type I IFN. IL-1β and type I IFN represent two major counterregulatory classes of inflammatory cytokines

that control the outcome of *M. tuberculosis* infection (31). Therefore, it is physiologically significant that the IL-1β signaling pathway negatively regulates the type I IFN signaling pathway during *M. tuberculosis* infection. Based on our data, we believe that activation of the AIM2 inflammasome protects the host from *M. tuberculosis*

FIGURE 5. ASC interacts with STING. (**A**) Immunoblot analysis of lysates from HEK293T cells that were cotransfected with the Flag vector or the Flag-STING vector and the HA-tagged vector, HA-ASC vector, or HA-Trim30α vector, followed by immunoprecipitation (IP) with anti-HA Ab and immunoblotting with anti-Flag Ab. (**B**) Immunoblot analysis of lysates of BMDCs that were mock treated or stimulated with poly(dA:dT) (1 μg/ml) or infected with BCG (multiplicity of infection = 10) for 6 h, followed by immunoprecipitation with anti-IgG Ab or anti-ASC Ab and immunoblotting with anti-STING Ab. (**C**) Confocal microscopy of MEFs that were transfected for 4 h with Flag-tagged STING and HA-tagged ASC and then mock treated or stimulated for 4 h with poly(dA:dT) (2 μg/ml). Immunofluorescence was performed using anti-HA Ab (red), anti-Flag Ab (green), and DAPI. (**D**) Immunoblot analysis of lysates from HEK293T cells that were cotransfected with Flag-STING and HA-tagged ASC or HA-tagged ASC truncations, followed by immunoprecipitation (IP) with anti-HA Ab and immunoblot analysis with anti-Flag Ab. (**E**) Immunoblot analysis of lysates from HEK293T cells cotransfected with HA-tagged ASC and Flag-STING or Flag-STING truncations, followed by immunoprecipitation (IP) with anti-HA Ab and immunoblot analysis with anti-Flag Ab. (**F**) Immunoblot analysis of lysates from HEK293T cells cotransfected with Myc-STING and Flag-TBK1 plus the HA vector or HA-ASC in gradient concentrations, followed by immunoprecipitation (IP) with anti-Flag Ab and immunoblot (IB) analysis with anti-Myc Ab. (**G**) Immunoblot analysis of lysates from HEK293T cells cotransfected with the Flag vector or Flag-TBK1 and HA-ASC, followed by immunoprecipitation (IP) with anti-HA Ab and immunoblot (IB) analysis with anti-Flag Ab. Data are representative of at least two independent experiments.
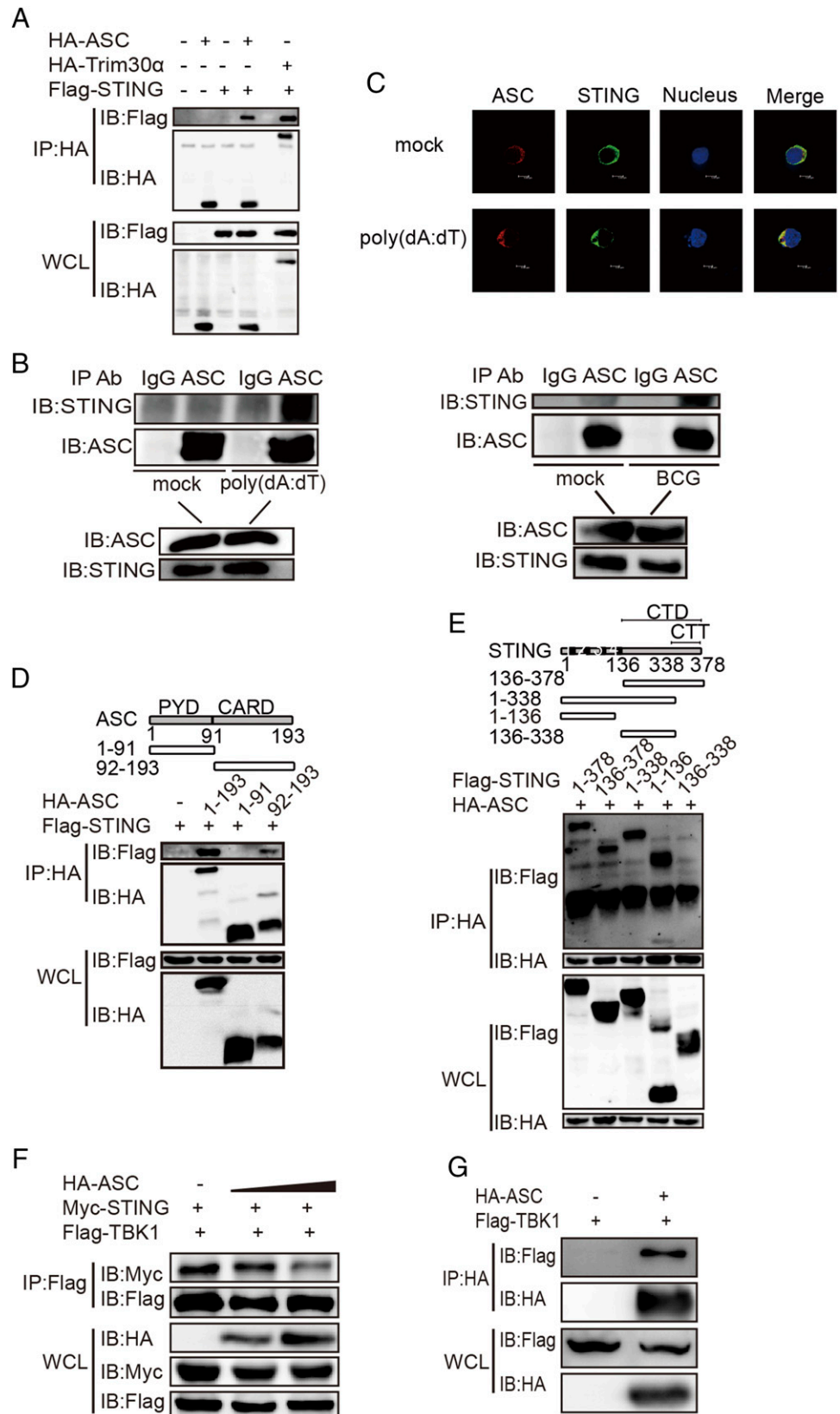
infection on one hand due to the induction of IL-1β and on the other hand due to downregulation of the type I IFN induction via cross-talk through ASC and STING interaction. Importantly, ASC expression is inversely correlated with the levels of IFN-β in PBMCs from TB patients, which emphasizes the clinical significance of the inhibitory role of ASC on IFN-β production.

Our results suggest that overproduction of type I IFNs leads to a reduced IFN-γ response during *M. tuberculosis* infection. The reciprocal IFN-β overproduction and IFN-γ depression during mycobacterial infection of AIM2$^{-/-}$ mice are consistent with the recent observation that IFN-β counterregulates the IFN-γ response upon infection with various *M. tuberculosis* strains (32).
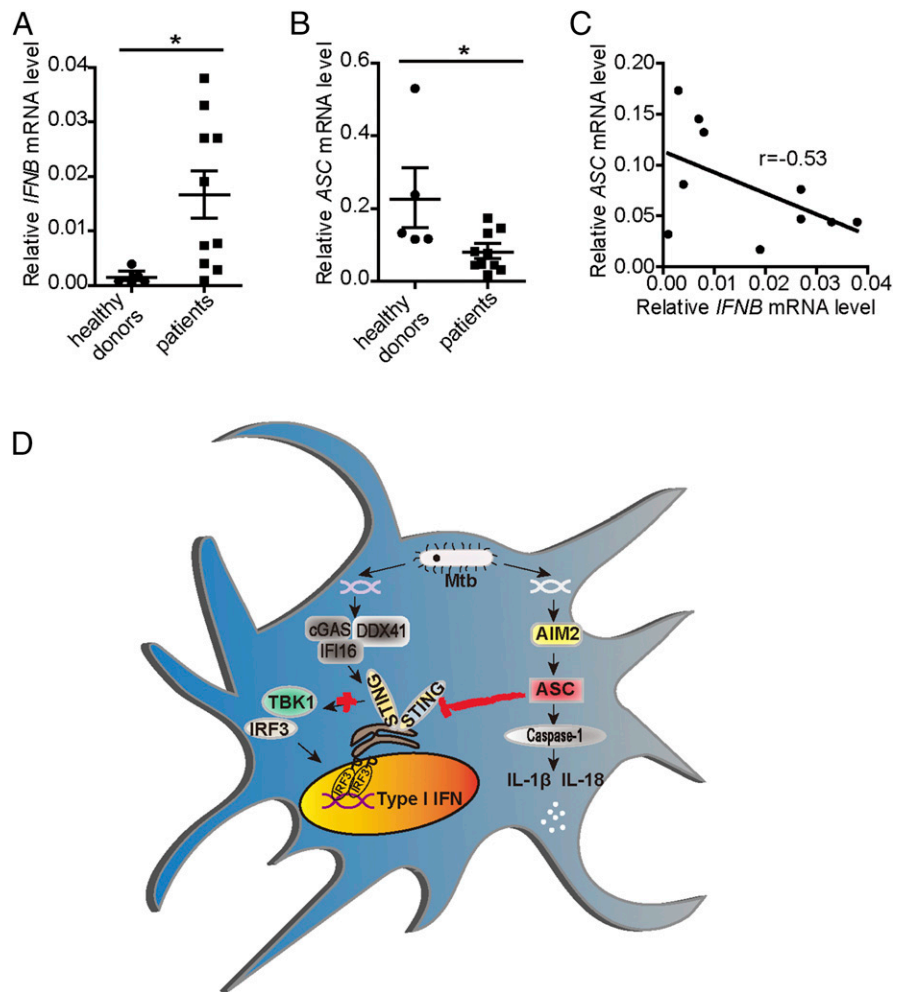
FIGURE 6. ASC expression is inversely correlated with IFN-β levels in PBMCs from TB patients. IFN-β and ASC expression in PBMCs from healthy donors ($n = 5$) and TB patients ($n = 10$) was examined by quantitative real-time PCR (qRT-PCR) (**A** and **B**), and their correlation was assessed with the Pearson test (**C**). (**D**) GD of *M. tuberculosis* can be recognized by the AIM2–IL-1β signaling pathway and the STING–type I IFN signaling pathway. Activated ASC interacts with STING and blocks the activation of downstream molecules TBK1 and IRF3, thus inhibiting the induction of IFN-β. The results are shown as mean ± SEM. *$p < 0.05$, Student *t* test.

Our data also support recent reports implicating that type I IFNs impair the Th1 response and inhibit IFN-γ–induced antimicrobial responses in macrophages/monocytes in virulent *M. tuberculosis* infection (13, 33).

In addition to the involvement of the AIM2 inflammasome and type I IFN signaling pathways in *M. tuberculosis* detection, another pathway is relevant: autophagy. Although one report suggested that AIM2-inhibited autophagy increases *M. bovis* survival in vitro (34), it is conceivable that activated ASC-mediated inhibition of IFN-β promotes resistance to *M. tuberculosis* in vivo. Therefore, additional studies are needed to elucidate the relationship among these three pathways. It will also be interesting to determine whether single nucleotide polymorphisms of ASC in TB patients correlate with changes in type I IFN. In addition to *M. tuberculosis*, another intracellular bacterium, *Listeria monocytogenes*, can induce the production of type I IFN and IL-1β in a DNA-dependent manner. Type I IFN is detrimental, and IL-1β is beneficial (35–37). Therefore, it would be helpful to determine whether the mechanism in our study applies to *L. monocytogenes* infection in vivo.

Intracellular DNAs that behave like classical PAMPs are involved in various innate immune response to viruses and intracellular bacteria and function during conditions of sterile inflammation, autoimmunity, and cancers (38). Because immune sensing of DNA plays critical roles in the early resistance to infections and subsequent bridge toward activation of adaptive immune responses, searching for DNA sensors that are involved in this process is especially important. Multiple DNA sensors,

including DAI, AIM2, RNA PolIII, LRRFIP1, DHX9/DHX36, IFI16, Ku70, DDX41, DNA-PK, MRE11, cGAS, and Rad50, have been identified, and their functions have been studied (39). However, how these DNA sensors act and influence each other remain unclear. The relationship that exists between the STING–type I IFN and AIM2 inflammasome signaling pathways, which are the two major pathways that are activated by DNA ligands, might be the most important to elucidate. A recently published article reported that inflammasome activation regulates type I IFN responses to DNA virus infection, which is presumably due to caspase-1–mediated cleavage of cGAS (40). Although our data showed that the production of IFN-β increased in Caspase-1$^{-/-}$ mice compared with WT mice, the extent of the increase was far below that of AIM2$^{-/-}$ and ASC$^{-/-}$ mice, which was consistent with previous studies (25). Therefore, it is likely that more than one mechanism is involved in the cross-talk between these two pathways. Given the different stimuli, cell types, and animal models that we used, it is possible that the dominant mechanisms underlying the regulatory effect of the AIM2 inflammasome on the type I IFN response differed based on the specific conditions used. And further studies are needed. Additionally, the blocked induction of downstream IFN-β by ASC interaction with STING prompts us to ask whether the STING pathway affects ASC-associated pathways, such as the AIM2 inflammasome and NLRP3 inflammasome signaling pathways. If so, exploring whether the effect is negative or positive and the pathological conditions in which this mechanism functions is meaningful.

Acknowledgments

Disclosures

References

1. World Health Organization. Global tuberculosis report 2015. Available at: http://www.tbonline.info/posts/2016/10/16/global-tb-report-2016/.
2. O'Garra, A., P. S. Redford, F. W. McNab, C. I. Bloom, R. J. Wilkinson, and M. P. Berry. 2013. The immune response in tuberculosis. *Annu. Rev. Immunol.* 31: 475–527.
3. Cai, X., Y. H. Chiu, and Z. J. Chen. 2014. The cGAS-cGAMP-STING pathway of cytosolic DNA sensing and signaling. *Mol. Cell* 54: 289–296.
4. Manzanillo, P. S., M. U. Shiloh, D. A. Portnoy, and J. S. Cox. 2012. *Mycobacterium tuberculosis* activates the DNA-dependent cytosolic surveillance pathway within macrophages. *Cell Host Microbe* 11: 469–480.
5. Collins, A. C., H. Cai, T. Li, L. H. Franco, X. D. Li, V. R. Nair, C. R. Scharn, C. E. Stamm, B. Levine, Z. J. Chen, and M. U. Shiloh. 2015. Cyclic GMP-AMP synthase is an innate immune DNA sensor for *Mycobacterium tuberculosis*. *Cell Host Microbe* 17: 820–828.
6. Wassermann, R., M. F. Gulen, C. Sala, S. G. Perin, Y. Lou, J. Rybniker, J. L. Schmid-Burgk, T. Schmidt, V. Hornung, S. T. Cole, and A. Ablasser. 2015. *Mycobacterium tuberculosis* differentially activates cGAS- and inflammasome-dependent intracellular immune responses through ESX-1. *Cell Host Microbe* 17: 799–810.
7. Watson, R. O., S. L. Bell, D. A. MacDuff, J. M. Kimmey, E. J. Diner, J. Olivas, R. E. Vance, C. L. Stallings, H. W. Virgin, and J. S. Cox. 2015. The cytosolic sensor cGAS detects *Mycobacterium tuberculosis* DNA to induce type I interferons and activate autophagy. *Cell Host Microbe* 17: 811–819.
8. McNab, F., K. Mayer-Barber, A. Sher, A. Wack, and A. O'Garra. 2015. Type I interferons in infectious disease. *Nat. Rev. Immunol.* 15: 87–103.
9. Berry, M. P., C. M. Graham, F. W. McNab, Z. Xu, S. A. Bloch, T. Oni, K. A. Wilkinson, R. Banchereau, J. Skinner, R. J. Wilkinson, et al. 2010. An interferon-inducible neutrophil-driven blood transcriptional signature in human tuberculosis. *Nature* 466: 973–977.
10. Cliff, J. M., J. S. Lee, N. Constantinou, J. E. Cho, T. G. Clark, K. Ronacher, E. C. King, P. T. Lukey, K. Duncan, P. D. Van Helden, et al. 2013. Distinct phases of blood gene expression pattern through tuberculosis treatment reflect modulation of the humoral immune response. *J. Infect. Dis.* 207: 18–29.
11. Maertzdorf, J., D. Repsilber, S. K. Parida, K. Stanley, T. Roberts, G. Black, G. Walzl, and S. H. Kaufmann. 2011. Human gene expression profiles of susceptibility and resistance in tuberculosis. *Genes Immun.* 12: 15–22.
12. Manca, C., L. Tsenova, S. Freeman, A. K. Barczak, M. Tovey, P. J. Murray, C. Barry, and G. Kaplan. 2005. Hypervirulent *M. tuberculosis* W/Beijing strains upregulate type I IFNs and increase expression of negative regulators of the Jak-Stat pathway. *J. Interferon Cytokine Res.* 25: 694–701.
13. Manca, C., L. Tsenova, A. Bergtold, S. Freeman, M. Tovey, J. M. Musser, C. E. Barry, III, V. H. Freedman, and G. Kaplan. 2001. Virulence of a *Mycobacterium tuberculosis* clinical isolate in mice is determined by failure to induce Th1 type immunity and is associated with induction of IFN-α/β. *Proc. Natl. Acad. Sci. USA* 98: 5752–5757.
14. Antonelli, L. R., A. Gigliotti Rothfuchs, R. Gonçalves, E. Roffê, A. W. Cheever, A. Bafica, A. M. Salazar, C. G. Feng, and A. Sher. 2010. Intranasal Poly-IC treatment exacerbates tuberculosis in mice through the pulmonary recruitment of a pathogen-permissive monocyte/macrophage population. *J. Clin. Invest.* 120: 1674–1682.
15. Bürckstümmer, T., C. Baumann, S. Blüml, E. Dixit, G. Dürnberger, H. Jahn, M. Planyavsky, M. Bilban, J. Colinge, K. L. Bennett, and G. Superti-Furga. 2009. An orthogonal proteomic-genomic screen identifies AIM2 as a cytoplasmic DNA sensor for the inflammasome. *Nat. Immunol.* 10: 266–272.
16. Fernandes-Alnemri, T., J. W. Yu, P. Datta, J. Wu, and E. S. Alnemri. 2009. AIM2 activates the inflammasome and cell death in response to cytoplasmic DNA. *Nature* 458: 509–513.
17. Hornung, V., A. Ablasser, M. Charrel-Dennis, F. Bauernfeind, G. Horvath, D. R. Caffrey, E. Latz, and K. A. Fitzgerald. 2009. AIM2 recognizes cytosolic dsDNA and forms a caspase-1-activating inflammasome with ASC. *Nature* 458: 514–518.
18. Yamada, H., S. Mizumo, R. Horai, Y. Iwakura, and I. Sugawara. 2000. Protective role of interleukin-1 in mycobacterial infection in IL-1 α/β double-knockout mice. *Lab. Invest.* 80: 759–767.
19. Juffermans, N. P., S. Florquin, L. Camoglio, A. Verbon, A. H. Kolk, P. Speelman, S. J. H. van Deventer, and T. van der Poll. 2000. Interleukin-1 signaling is essential for host defense during murine pulmonary tuberculosis. *J. Infect. Dis.* 182: 902–908.
20. Saiga, H., S. Kitada, Y. Shimada, N. Kamiyama, M. Okuyama, M. Makino, M. Yamamoto, and K. Takeda. 2012. Critical role of AIM2 in *Mycobacterium tuberculosis* infection. *Int. Immunol.* 24: 637–644.
21. Mariathasan, S., K. Newton, D. M. Monack, D. Vucic, D. M. French, W. P. Lee, M. Roose-Girma, S. Erickson, and V. M. Dixit. 2004. Differential activation of the inflammasome by caspase-1 adaptors ASC and Ipaf. *Nature* 430: 213–218.
22. Wang, Y., Q. Lian, B. Yang, S. Yan, H. Zhou, L. He, G. Lin, Z. Lian, Z. Jiang, and B. Sun. 2015. TRIM30α is a negative-feedback regulator of the intracellular DNA and DNA virus-triggered response by targeting STING. *PLoS Pathog.* 11: e1005012.
23. Waeckerle-Men, Y., N. Bruffaerts, Y. Liang, F. Jurion, P. Sander, T. M. Kündig, K. Huygen, and P. Johansen. 2013. Lymph node targeting of BCG vaccines amplifies CD4 and CD8 T-cell responses and protection against *Mycobacterium tuberculosis*. *Vaccine* 31: 1057–1064.
24. Platanias, L. C. 2005. Mechanisms of type-I- and type-II-interferon-mediated signalling. *Nat. Rev. Immunol.* 5: 375–386.
25. Corrales, L., S. R. Woo, J. B. Williams, S. M. McWhirter, T. W. Dubensky, Jr., and T. F. Gajewski. 2016. Antagonism of the STING pathway via activation of the AIM2 inflammasome by intracellular DNA. *J. Immunol.* 196: 3191–3198.
26. Jin, T., A. Perry, J. Jiang, P. Smith, J. A. Curry, L. Unterholzner, Z. Jiang, G. Horvath, V. A. Rathinam, R. W. Johnstone, et al. 2012. Structures of the HIN domain:DNA complexes reveal ligand binding and activation mechanisms of the AIM2 inflammasome and IFI16 receptor. *Immunity* 36: 561–571.
27. Sun, L., J. Wu, F. Du, X. Chen, and Z. J. Chen. 2013. Cyclic GMP-AMP synthase is a cytosolic DNA sensor that activates the type I interferon pathway. *Science* 339: 786–791.
28. Unterholzner, L., S. E. Keating, M. Baran, K. A. Horan, S. B. Jensen, S. Sharma, C. M. Sirois, T. Jin, E. Latz, T. S. Xiao, et al. 2010. IFI16 is an innate immune sensor for intracellular DNA. *Nat. Immunol.* 11: 997–1004.
29. Zhang, Z., B. Yuan, M. Bao, N. Lu, T. Kim, and Y. J. Liu. 2011. The helicase DDX41 senses intracellular DNA mediated by the adaptor STING in dendritic cells. *Nat. Immunol.* 12: 959–965.
30. Tanaka, Y., and Z. J. Chen. 2012. STING specifies IRF3 phosphorylation by TBK1 in the cytosolic DNA signaling pathway. *Sci. Signal.* 5: ra20.
31. Mayer-Barber, K. D., B. B. Andrade, S. D. Oland, E. P. Amaral, D. L. Barber, J. Gonzales, S. C. Derrick, R. Shi, N. P. Kumar, W. Wei, et al. 2014. Host-directed therapy of tuberculosis based on interleukin-1 and type I interferon crosstalk. *Nature* 511: 99–103.
32. Dey, B., R. J. Dey, L. S. Cheung, S. Pokkali, H. Guo, J.-H. Lee, and W. R. Bishai. 2015. A bacterial cyclic dinucleotide activates the cytosolic surveillance pathway and mediates innate resistance to tuberculosis. *Nat. Med.* 21: 401–406.
33. Ordway, D., M. Henao-Tamayo, M. Harton, G. Palanisamy, J. Troudt, C. Shanley, R. J. Basaraba, and I. M. Orme. 2007. The hypervirulent *Mycobacterium tuberculosis* strain HN878 induces a potent TH1 response followed by rapid down-regulation. *J. Immunol.* 179: 522–531.
34. Liu, C., R. Yue, Y. Yang, Y. Cui, L. Yang, D. Zhao, and X. Zhou. 2016. AIM2 inhibits autophagy and IFN-β production during *M. bovis* infection. *Oncotarget* 7: 46972–46987.
35. Auerbuch, V., D. G. Brockstedt, N. Meyer-Morse, M. O'Riordan, and D. A. Portnoy. 2004. Mice lacking the type I interferon receptor are resistant to *Listeria monocytogenes*. *J. Exp. Med.* 200: 527–533.
36. Carrero, J. A., B. Calderon, and E. R. Unanue. 2004. Type I interferon sensitizes lymphocytes to apoptosis and reduces resistance to *Listeria* infection. *J. Exp. Med.* 200: 535–540.
37. O'Connell, R. M., S. K. Saha, S. A. Vaidya, K. W. Bruhn, G. A. Miranda, B. Zarnegar, A. K. Perry, B. O. Nguyen, T. F. Lane, T. Taniguchi, et al. 2004. Type I interferon production enhances susceptibility to *Listeria monocytogenes* infection. *J. Exp. Med.* 200: 437–445.
38. Hemmi, H., O. Takeuchi, T. Kawai, T. Kaisho, S. Sato, H. Sanjo, M. Matsumoto, K. Hoshino, H. Wagner, K. Takeda, and S. Akira. 2000. A Toll-like receptor recognizes bacterial DNA. *Nature* 408: 740–745.
39. Unterholzner, L. 2013. The interferon response to intracellular DNA: why so many receptors? *Immunobiology* 218: 1312–1321.
40. Wang, Y., X. Ning, P. Gao, S. Wu, M. Sha, M. Lv, X. Zhou, J. Gao, R. Fang, G. Meng, et al. 2017. Inflammasome activation triggers caspase-1-mediated cleavage of cGAS to regulate responses to DNA virus infection. *Immunity* 46: 393–404.

Corrections

Yan, S., H. Shen, Q. Lian, W. Jin, R. Zhang, X. Lin, W. Gu, X. Sun, G. Meng, Z. Tian, Z. W. Chen, and B. Sun. 2018. Deficiency of the AIM2–ASC signal uncovers the STING-driven overreactive response of type I IFN and reciprocal depression of protective IFN-γ immunity in mycobacterial infection. *J. Immunol.* 200: 1016–1026.

There were errors in Zheng W. Chen's affiliations as originally published. The corrected author line and affiliations are shown below, as is the author contribution footnote. The author line and affiliations have also been corrected in the online version of the article, which now differs from the print version as originally published.

Shanshan Yan,[*,†] Hongbo Shen,[‡,1] Qiaoshi Lian,[†,§] Wenlong Jin,[‡] Ronghua Zhang,[†] Xuan Lin,[‡] Wangpeng Gu,[*,†] Xiaoyu Sun,[‡] Guangxun Meng,[‡] Zhigang Tian,[*] Zheng W. Chen,[¶,1] and Bing Sun[†,1]

*School of Life Sciences, University of Science and Technology of China, Hefei 230022, China; [†]State Key Laboratory of Cell Biology, CAS Center for Excellence in Molecular Cell Science, Shanghai Institute of Biochemistry and Cell Biology, Chinese Academy of Sciences, University of Chinese Academy of Sciences, Shanghai 200031, China; [‡]CAS Key Laboratory of Molecular Virology and Immunology, Institute Pasteur of Shanghai, Chinese Academy of Sciences, Shanghai 200031, China; [§]University of Chinese Academy of Sciences, Beijing 100049, China; and [¶]Department of Microbiology and Immunology, Center for Primate Biomedical Research, University of Illinois College of Medicine, Chicago, IL 60612

[1]H.S., Z.W.C., and B.S. are the senior authors and contributed equally to this work.

www.jimmunol.org/cgi/doi/10.4049/jimmunol.1901370